NASA/TM–20210020762

Numerical Simulation of Pressure-induced Separation of Turbulent Flat-plate Boundary Layers: Definition and Overview of New Cases with Suction-only Transpiration and a Step in Reynolds Number

Gary Neil Coleman
Langley Research Center, Hampton, Virginia

September 2021

NASA STI Program... in Profile

Since its founding, NASA has been dedicated to the advancement of aeronautics and space science. The NASA scientific and technical information (STI) program plays a key part in helping NASA maintain this important role.

The NASA STI Program operates under the auspices of the Agency Chief Information Officer. It collects, organizes, provides for archiving, and disseminates NASA's STI. The NASA STI Program provides access to the NASA Aeronautics and Space Database and its public interface, the NASA Technical Report Server, thus providing one of the largest collection of aeronautical and space science STI in the world. Results are published in both non-NASA channels and by NASA in the NASA STI Report Series, which includes the following report types:

- TECHNICAL PUBLICATION. Reports of completed research or a major significant phase of research that present the results of NASA programs and include extensive data or theoretical analysis. Includes compilations of significant scientific and technical data and information deemed to be of continuing reference value. NASA counterpart of peer-reviewed formal professional papers, but having less stringent limitations on manuscript length and extent of graphic presentations.
- TECHNICAL MEMORANDUM. Scientific and technical findings that are preliminary or of specialized interest, e.g., quick release reports, working papers, and bibliographies that contain minimal annotation. Does not contain extensive analysis.
- CONTRACTOR REPORT. Scientific and technical findings by NASA-sponsored contractors and grantees.
- CONFERENCE PUBLICATION. Collected papers from scientific and technical conferences, symposia, seminars, or other meetings sponsored or co-sponsored by NASA.
- SPECIAL PUBLICATION. Scientific, technical, or historical information from NASA programs, projects, and missions, often concerned with subjects having substantial public interest.
- TECHNICAL TRANSLATION. English-language translations of foreign scientific and technical material pertinent to NASA's mission.

Specialized services also include organizing and publishing research results, distributing specialized research announcements and feeds, providing information desk and personal search support, and enabling data exchange services.

For more information about the NASA STI Program, see the following:

- Access the NASA STI program home page at `http://www.sti.nasa.gov`
- E-mail your question to `help@sti.nasa.gov`
- Phone the NASA STI Information Desk at 757-864-9658
- Write to:
  NASA STI Information Desk
  Mail Stop 148
  NASA Langley Research Center
  Hampton, VA 23681-2199

NASA/TM–20210020762

Numerical Simulation of Pressure-induced Separation of Turbulent Flat-plate Boundary Layers: Definition and Overview of New Cases with Suction-only Transpiration and a Step in Reynolds Number

Gary Neil Coleman
Langley Research Center, Hampton, Virginia

National Aeronautics and
Space Administration

Langley Research Center
Hampton, Virginia 23681-2199

September 2021

Errata

Issued January 2022 for

NASA-TM-20210020762

Numerical Simulation of Pressure-induced Separation of Turbulent Flat-plate Boundary Layers:
Definition and Overview of New Cases with Suction-only Transpiration and a Step in Reynolds Number

Gary Neil Coleman

Summary of changes:

Figure 7 and associated text were added.

Acknowledgments

This work was sponsored by the NASA Transformational Tools and Technologies (TTT) Project of the Transformative Aeronautics Concepts Program under the Aeronautics Research Mission Directorate. Computations were performed on resources provided by the NASA Advanced Supercomputing (NAS) Division. The author is grateful to Dr. David Scott, for the UK/EPSRC-sponsored code development, and Drs. Christopher Rumsey and Philippe Spalart, for their timely advice and comments.

Available from:

NASA STI Program / Mail Stop 148
NASA Langley Research Center
Hampton, VA 23681-2199
Fax: 757-864-6500

Abstract

Results from two new direct numerical simulations (DNSs) are added to the database described in Coleman, Rumsey & Spalart (2018) (henceforth CRS18), and available at the NASA TMR website (https://turbmodels.larc.nasa.gov). The new flows, Cases D and E, are similar to the earlier ones (Cases A–C) in that a transpiration profile above a flat plate creates a prolonged adverse pressure gradient (APG) that drives a canonical turbulent zero-pressure-gradient (ZPG), flat-plate boundary layer towards separation; they differ in that for the new cases (1) the APG is not followed by a favorable gradient (FPG), since only suction transpiration is employed, and (2) the mean shear stress does not cross zero, so that the width of the mean bubble, strictly defined, is zero. However, the probability of reversed skin friction exceeds 49%. The motivation was to produce a flow more akin to technological flows, including shock-boundary-layer interaction, with a gradual turbulence-controlled recovery. One of the new simulations is also at a significantly higher Reynolds number than the earlier flows.

Description of new DNS

The fully turbulent incompressible ZPG boundary layer over a flat no-slip surface is subject to streamwise (x) pressure gradients induced by a transpiration profile $V_{\rm top}(x)$ through a virtual parallel streamwise-spanwise (x-z) plane offset a fixed wall-normal distance $y = Y$ from the no-slip surface. The strength and duration of the pressure gradients are controlled by the maximum velocity $V_{\rm max}$ and length-scale σ; for Cases D and E (cf. (2.1) of CRS18),

$$V_{\rm top}(x) = V_{\rm max} \exp\left(-\left[\frac{x - x_0}{\sigma}\right]^2\right) + \varphi_{\rm top}\, g(x) + \Phi(x), \qquad (1)$$

where x_0 sets the location of the peak $V_{\rm top}$, $\varphi_{\rm top}$ is a small 'bleed' velocity, adjusted to offset the blockage in the (nominally) ZPG regions upstream of separation, and thereby produce $\mathrm{d}P/\mathrm{d}x \approx 0$ along the wall there; the bleed velocity is constant for $x < x_\varphi$ and zero for $x > x_\varphi$, since $g(x) = 0.5\,(1 - \mathrm{erf}\,((x - x_\varphi)/\sigma_\varphi))$. We use $x_\varphi = 15.35$ and $\sigma_\varphi = \sigma/10$ for both cases. The transpiration is very similar to that of Alam & Sandham (2000) and Spalart & Strelets (2000), although both those studies had a laminar incoming boundary layer, and Wu, Meneveau & Mittal (2020). The inflow/outflow boundary conditions are imposed by the fringe-zone treatment described in CRS18, which allows a fully spectral spatial scheme to accommodate the spatially developing, nonparallel flow. The fringe parameters given in Table 3 of CRS18 (x_1, V_2, y_α, Υ, y_β), along with (A1) and (A2) of CRS18, are also used for Cases D and E. The last term in (1) maintains zero net mass flux across the $y = Y$ plane, by injecting mass into the fringe zones (and only there): $\Phi(x) = -(V_{\rm max}\sigma/x_1 + \varphi_{\rm top} x_\varphi/\sqrt{\pi} x_1)\, H(x)$, where $H(x) = \exp\left(-(x/x_1)^2\right) + \exp\left(-((x - \Lambda_x)/x_2)^2\right)$. Other numerical details are as given in CRS18.

Table 1. Case parameters.

Case	$U_\infty Y/\nu$	$V_{\max}/U_\infty$	x_0/Y	σ/Y	$\varphi_{\text{top}}/U_\infty$
D	80 000	0.125	12.762	2.407	0.0032
E	180 000	0.125	12.762	2.407	0.0032

The cases are summarized in Table 1. Case D is at the same Reynolds number as the previous Case C, whereas the Reynolds number of Case E is more than twice as high. Figure 1 illustrates the qualitative differences between the new suction-only cases (dashed and solid curves) and the earlier APG/FPG flows (the chain-dotted curves are from Case C of CRS18). Note the weak APG (replacing a strong FPG), and continued growth of the boundary layer, downstream of the $V_{\text{top}} > 0$ region. Mean-flow contours and streamlines for Case E are shown in Figure 2. The 'hotspot' in the Reynolds shear stress $-\overline{u'v'}$ near $x = 21$ (Figure 2*b*) is qualitatively similar to that observed in the NASA wall-mounted hump experiment (Greenblatt et al. 2006a,b; Naughton et al. 2006), although here it is milder: compared to the peak value found in the experiment of about $0.03\,(\Delta U)^2$ (where ΔU is the velocity difference across the effective shear layer within which the hotspot is embedded), the Case E equivalent is $-\overline{u'v'} \approx 0.01\,(\Delta U)^2$. The latter is similar to the value in a plane mixing layer, and therefore there is some expectation that turbulence models may reproduce it, provided the growth from the much lower levels typical of boundary layers is rapid enough.

We interpret the $x/Y = 7.5$ station as the ZPG reference states. At these locations, the Case D and E flows both agree well with ZPG boundary-layer results from DNS and experiment, in terms of mean velocity at momentum thickness Reynolds numbers of 1479 and 3069 (Figure 3). The profiles of near-wall turbulence kinetic energy and terms in its budget (neither shown) also agree well with Schlatter & Örlü's (2010) DNS at comparable R_θ. In the outer layer, the Case E profile is somewhat more energetic than the pure ZPG DNS benchmark at the same y^+ location (cf. Figure 6 of CRS18, regarding Case C).

The numerical parameters are summarized in Table 2; in general they meet the standard required of a DNS (cf. § 2.2 of CRS18): the spatial resolution is quite close to that used in CRS18, and all scales are fully captured throughout most of the domain. The exception (as in CRS18) is the marginal accommodation of the residual vorticity near the top wall, associated with the layer thickness approaching the transpiration plane – which in CRS18 resulted in minor near-wall oscillation (Gibbs phenomenon) in the profiles above the separation bubble (see Figure 4 of CRS18). The present Figure 4 shows mean and root-mean-square (RMS) fluctuations of vorticity at several x-stations. At upstream stations ($x/Y = 7.5$ shown here), the profiles decay cleanly to zero well below the upper, transpiration boundary. But starting near $x/Y = 15$ and extending downstream ($x/Y = 15$ and 23 are shown), nonzero levels of $\overline{\varpi}_z$ and $\overline{\omega_i'\omega_i'}^{\,1/2}$ are evident near the upper boundary. These nonzero levels extend from near $x/Y = 15$ (where the skin friction is smallest) until the outflow station, where for both new cases the RMS vertical velocity fluc-

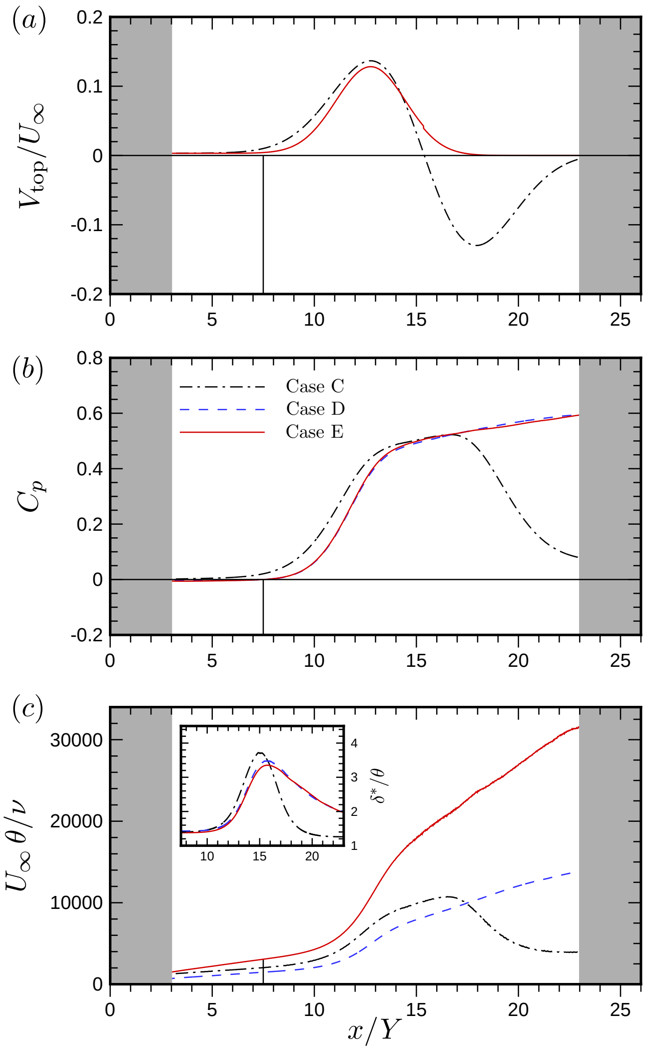

Figure 1. Streamwise variation of (a) transpiration profile along $y = Y$, (b) mean wall pressure and (c) momentum-thickness Reynolds number and shape factor. Case D and E results are identical in (a). Vertical lines mark the assumed ZPG reference station for Cases D and E. Shaded rectangles (approximately $3Y$ wide) indicate regions where the fringe/inflow-treatment is active for Cases D and E. (For Case C, the effective fringe regions are each approximately 2Ywide, since the boundary layer to which the fringe forcing is applied is thinner in that flow, due to its FPG downstream of separation.)

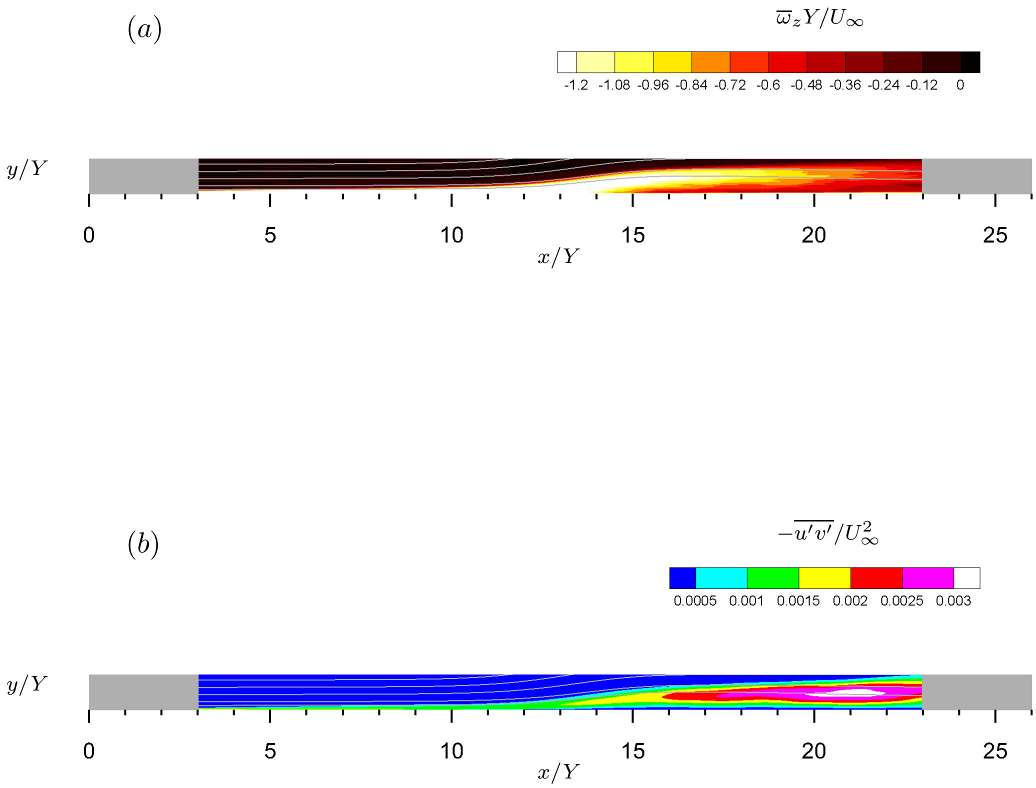

Figure 2. Contours of mean streamlines and (a) spanwise vorticity $\overline{\omega}_z$ and (b) Reynolds shear stress $-\overline{u'v'}$ for Case E. Shaded/grey regions at in/outflow of domain are fringe zones.

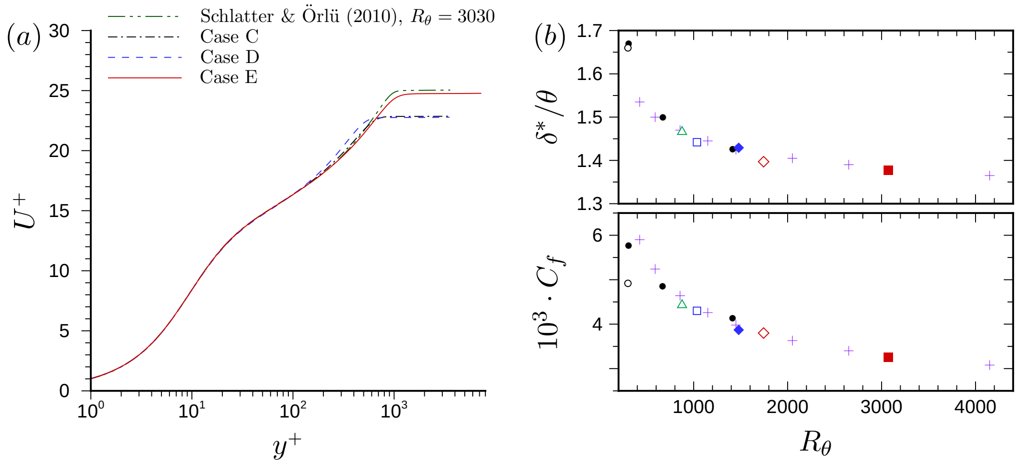

Figure 3. (a) Mean-velocity in ZPG regions. (b) Skin-friction and shape factor: +, Coles (1962); •, Spalart (1988); ○, SC97; □, Case A; △, Case B; ◇, Case C; ♦, Case D; ■, Case E.

Table 2. Numerical parameters. Dealiasing is enforced by defining the number of quadrature/collocation points, N_x, N_y and N_z, such that they are related to the number of streamwise, wall-normal and spanwise Galerkin spectral expansion coefficients, respectively, by $M_x = 2N_x/3$, $M_y = (2N_y - 9)/3$ and $M_z = 2N_z/3$. Spatial resolution is quantified in terms of the quadrature grid, such that $\Delta x = \Lambda_x/N_x$ and $\Delta z = \Lambda_z/N_z$, where Λ_x and Λ_z are respectively streamwise and spanwise domain periods. The distance y_{10} is that of the tenth wall-normal quadrature point from the bottom of the domain (with $y_1 = 0$). Wall units, e.g., $\Delta x^+ = \Delta x\, u_\tau/\nu$ and $y_{10}^+ = y_{10}\, u_\tau/\nu$, are based on skin friction at $x/Y = 3$.

Case	Λ_x/Y	Λ_z/Y	N_x	Δx^+	N_y	y_{10}^+	N_z	Δz^+
C	26.0	4.0	7680	12.3	240	4.6	2560	5.7
D	26.0	4.0	7680	13.4	240	5.0	2560	6.2
E	26.0	4.0	18 432	11.6	320	5.8	6400	5.1

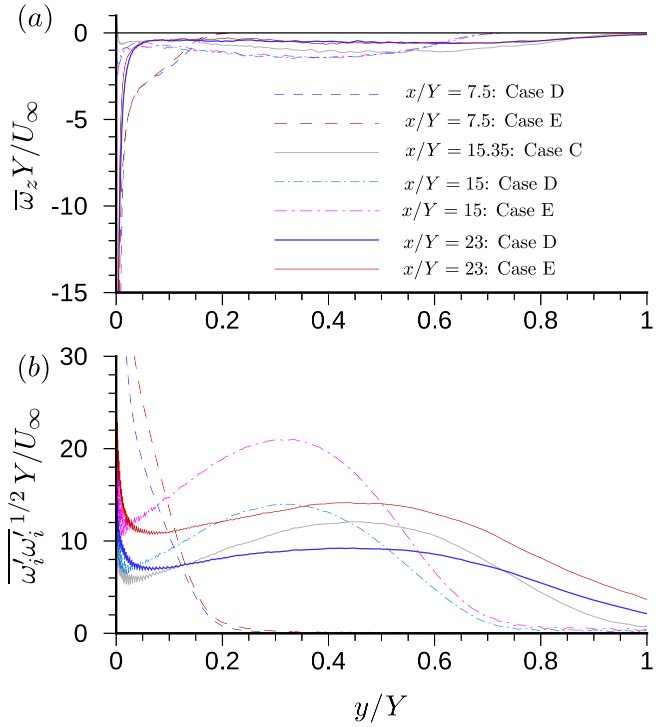

Figure 4. Profiles of (a) mean spanwise vorticity $\overline{\omega}_z$ and (b) root-mean-square vorticity fluctuations $\overline{\omega_i'\omega_i'}^{\,1/2}$.

tuations (not shown) are approximately $0.025U_\infty$ at $y = Y$, compared with a peak value of about 0.064 (near $y = 0.45Y$). As was true for Cases A, B, and C, although the vorticity oscillations are relatively small, this implies certain statistics (such as the dissipation term in the turbulence-kinetic-energy budget) should be viewed with caution in the affected regions, downstream of the minimum skin-friction station.

The parameters of the transpiration profile were adjusted to drive the layer just to the point of mean separation, near $x/Y = 15$, before allowing the flow to recover under nominally ZPG conditions before exiting/reentering the domain through the fringe zones (Figures 1 and 5a). The mean-velocity profile evolves in the downstream $V_{\text{top}} = 0$ region such that a mild APG ensues (see the shape-factor δ^*/θ profile in Figure 1c). Despite the skin friction just 'kissing' $C_f = 0$ before growing again, the structure of the near-wall turbulence under the APG is qualitatively similar to flows for which a finite separation bubble forms. This can been seen by comparing Figure 6 with Figure 1d of CRS18. This underlines the oft-made observation that the flow does not fundamentally change once it passes the mean $C_f = 0$ location, which also closely corresponds to the 50% back-flow station (Figure 5b). Figure 5b also demonstrates the tendency for the small but nonzero number of instantaneous reversed-flow events at the wall under the ZPG layer (e.g. at $x/Y = 7.5$) to increase with Reynolds number (Spalart 1988).

Statistics were gathered by averaging over z and in time, involving 381 and 763 x-y fields over periods of 35.1 and $16.35Y/U_\infty$, respectively, for Cases D and

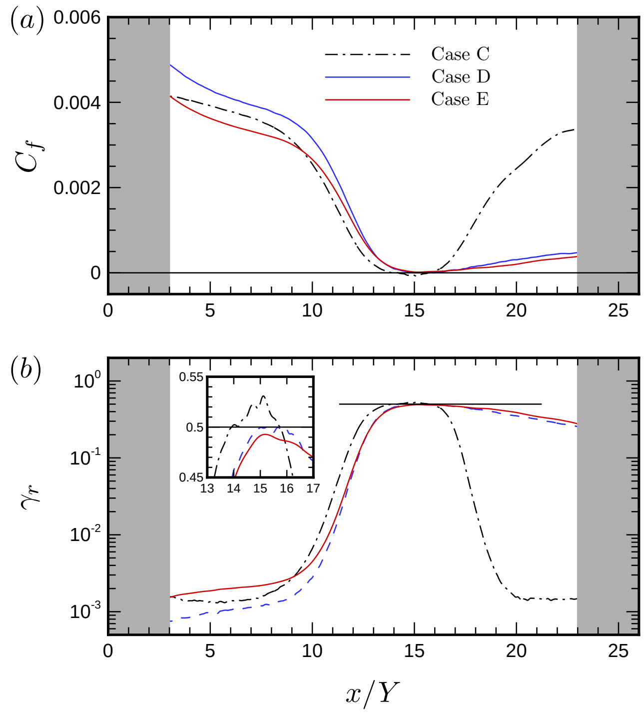

Figure 5. (a) Skin-friction $C_f = \tau_w / \frac{1}{2} \rho U_\infty^2$ and (b) fraction of reversed wall shear γ_r. Horizontal lines in (b) denote $\gamma_r = 0.50$ threshold.

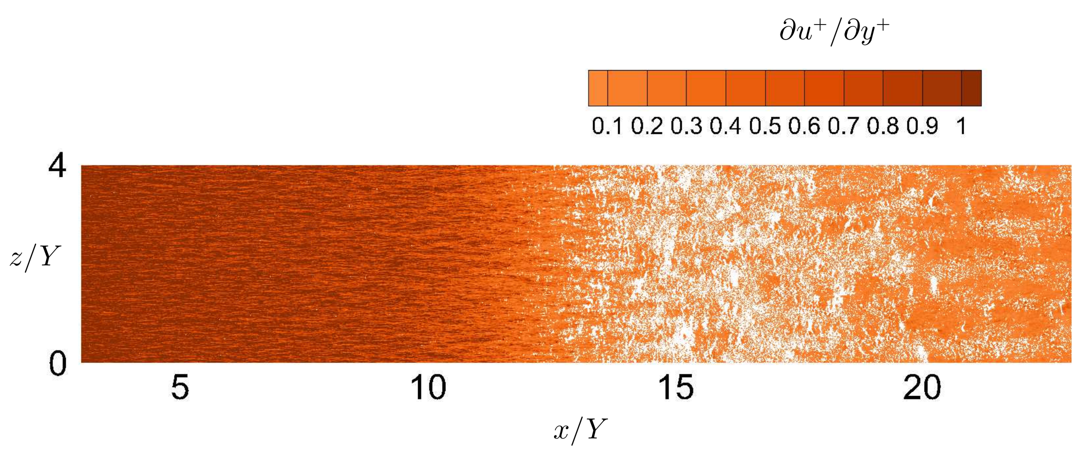

Figure 6. Contours of instantaneous surface shear stress for Case D. White contours denote $\partial u / \partial y < 0$.

(*a*)

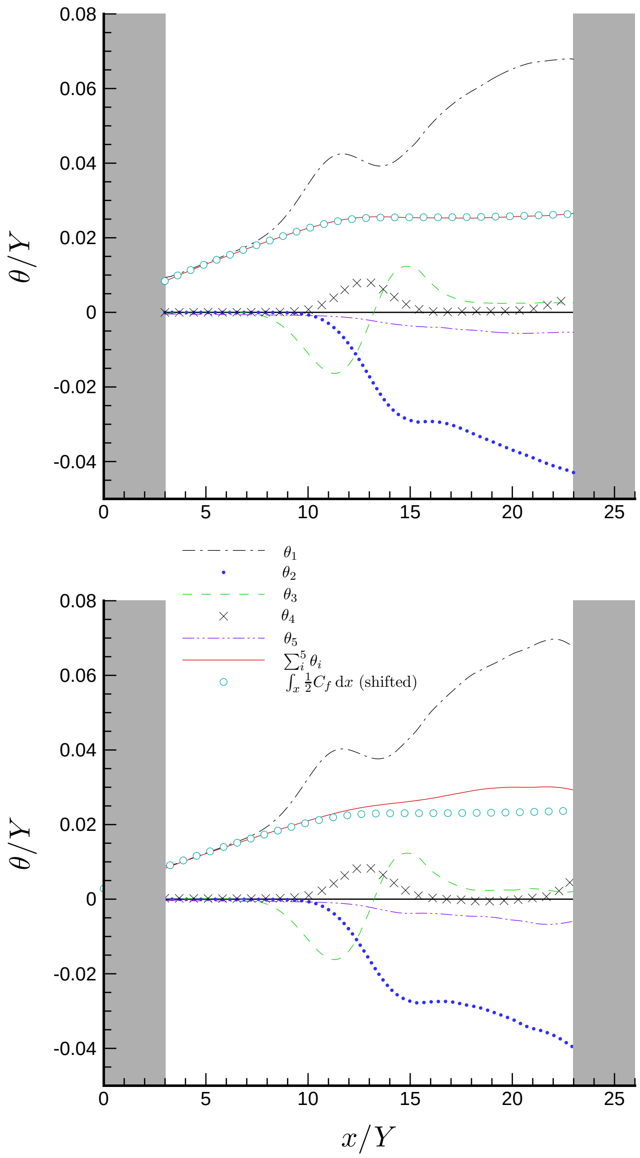

Figure 7. Integrated momentum balance for (*a*) Case D and (*b*) Case E. See Appendix C of CRS18 for definitions.

E (respectively corresponding to 1.35 and 0.6 domain-flow-through times Λ_x/U_∞). Some quantities were also locally averaged in x. The z- and t-averaged data are available from the NASA Turbulence Modeling Resource (TMR) website.[1]

Computations were done on the NASA Advanced Supercomputing (NAS) Division's Aitken AMD Rome system, on 4096 cores. A total of about 245,000 (Case D) and 2,561,000 (Case E) CPU-core-hours were utilized during the statistics-gatherings phase of the computations. The resulting x-variations of the y-integrated momentum balances are shown in figure 7. For Case D, the balance is very good at each streamwise station. For Case E, on the other hand, the imbalance grows slowly with streamwise distance (primarily because θ_1, the term proportional to the standard momentum thickness, is too large), such that the sum of the $\theta_1 - \theta_5$ thicknesses (see Appendix C of CRS18) differs by more than 1% of the skin-friction integral downstream of $x/Y \approx 8.75$, where $\Pi^+ = [\mathrm{d}(P/\rho)/\mathrm{d}x]/[u_\tau^3/\nu] \approx 0.001$. Consequently, the uncertainty of the higher-Reynolds-number, Case E data is lowest in the ZPG region and early stages of the ZPG-to-APG transition, where the trajectory towards separation is first established.

Closing comments

Taken in tandem with CRS18, these new DNS data are expected to aid understanding of canonical smooth-body separation driven by APG. The new data provide a different type of recovery from separation (gentle APG rather than FPG), and also include two different Reynolds numbers.

References

Alam, M. & Sandham, N. D. 2000 Direct numerical simulation of 'short' laminar separation bubbles with turbulent reattachment. *J. Fluid Mech.* **410**, 1–28.

Coles, D. E. 1962 The turbulent boundary layer in a compressible fluid. *Rand Rep.* R403-PR, ARC 24473: Appendix A: A manual of experimental practice for low-speed flow.

Greenblatt, D., Paschal, K. B., Yao, C.-S., Harris, J., Schaeffler, N. W. & Washburn, A. E. 2006a Experimental investigation of separation control Part 1: Baseline and steady suction. *AIAA J.* **44**(12), 2820–2830.

Greenblatt, D., Paschal, K. B., Yao, C.-S. & Harris, J. 2006b Experimental investigation of separation control Part 2: Zero mass-flux oscillatory blowing. *AIAA J.* **44**(12), 2831–2845.

Naughton, J. W., Viken, S. A. & Greenblatt, D. 2006 Skin-friction measurements on the NASA hump model. *AIAA J.* **44**(6), 1255–1265.

Schlatter, P. & Örlü 2010 Assessment of direct numerical simulation data of turbulent boundary layers. *J. Fluid Mech.* **659**, 116–126.

[1] https://turbmodels.larc.nasa.gov .

Spalart, P.R. 1988 Direct simulation of a turbulent boundary layer up to $R_\theta = 1410$. *J. Fluid Mech.* **187**, 61–98.

Spalart, P.R. & Strelets, M. Kh. 2000 Mechanisms of transition and heat transfer in a separation bubble. *J. Fluid Mech.* **403**, 329–349.

Wu, W., Meneveau, C. & Mittal, R. 2020 Spatio-temporal dynamics of turbulent separation bubbles. *J. Fluid Mech.* **883**, A45.

REPORT DOCUMENTATION PAGE		*Form Approved OMB No. 0704–0188*

1. REPORT DATE *(DD-MM-YYYY)*	**2. REPORT TYPE**	**3. DATES COVERED** *(From - To)*
01-09-2021	Technical Memorandum	

4. TITLE AND SUBTITLE
Numerical Simulation of Pressure-induced Separation of Turbulent Flat-plate Boundary Layers: Definition and Overview of New Cases with Suction-only Transpiration and a Step in Reynolds Number

5a. CONTRACT NUMBER

5b. GRANT NUMBER

5c. PROGRAM ELEMENT NUMBER

6. AUTHOR(S)
Gary Neil Coleman

5d. PROJECT NUMBER

5e. TASK NUMBER

5f. WORK UNIT NUMBER
109492.02.07.05.01

7. PERFORMING ORGANIZATION NAME(S) AND ADDRESS(ES)
NASA Langley Research Center
Hampton, Virginia 23681-2199

8. PERFORMING ORGANIZATION REPORT NUMBER
L–

9. SPONSORING/MONITORING AGENCY NAME(S) AND ADDRESS(ES)
National Aeronautics and Space Administration
Washington, DC 20546-0001

10. SPONSOR/MONITOR'S ACRONYM(S)
NASA

11. SPONSOR/MONITOR'S REPORT NUMBER(S)
NASA/TM–2021–0020762

12. DISTRIBUTION/AVAILABILITY STATEMENT
Unclassified-Unlimited
Subject Category
Availability: NASA STI Program (757) 864-9658

13. SUPPLEMENTARY NOTES
An electronic version can be found at http://ntrs.nasa.gov.
A revision was made to this document January 2022.

14. ABSTRACT
Results from two new direct numerical simulations (DNSs) are added to the database described in Coleman, Rumsey & Spalart (2018) (henceforth CRS18), and available at the NASA TMR website (https://turbmodels.larc.nasa.gov). The new flows, Cases D and E, are similar to the earlier ones (Cases A–C) in that a transpiration profile above a flat plate creates a prolonged adverse pressure gradient (APG) that drives a canonical turbulent zero-pressure-gradient (ZPG), flat-plate boundary layer towards separation; they differ in that for the new cases (1) the APG is not followed by a favorable gradient (FPG), since only suction transpiration is employed, and (2) the mean shear stress does not cross zero, so that the width of the mean bubble, strictly defined, is zero. However, the probability of reversed skin friction exceeds 49%. The motivation was to produce a flow more akin to technological flows, including shock-boundary-layer interaction, with a gradual turbulence-controlled recovery. One of the new simulations is also at a significantly higher Reynolds number than the earlier flows.

15. SUBJECT TERMS
Direct numerical simulation, turbulent boundary layer, adverse pressure gradient, separation

16. SECURITY CLASSIFICATION OF: a. REPORT	b. ABSTRACT	c. THIS PAGE	**17. LIMITATION OF ABSTRACT**	**18. NUMBER OF PAGES**	**19a. NAME OF RESPONSIBLE PERSON**
U	U	U	UU		STI Information Desk (help@sti.nasa.gov)
					19b. TELEPHONE NUMBER ***(Include area code)*** (757) 864-9658